Polymer 50 (2009) 578–584

Contents lists available at ScienceDirect

Polymer

journal homepage: www.elsevier.com/locate/polymer

The melting process and the rigid amorphous fraction of *cis*-1,4-polybutadiene

Maria Laura Di Lorenzo*

Istituto di Chimica e Tecnologia dei Polimeri (CNR) – c/o Comprensorio Olivetti – Via Campi Flegrei, 34–80078 Pozzuoli (NA), Italy

ARTICLE INFO

Article history:
Received 13 October 2008
Received in revised form
29 October 2008
Accepted 14 November 2008
Available online 25 November 2008

Keywords:
Multiple melting
Rigid amorphous fraction
Polybutadiene

ABSTRACT

A thorough analysis of the melting behavior of *cis*-1,4-polybutadiene (*cis*-PBD) is detailed in this contribution. Isothermal crystallization at −26 °C, followed by cooling, provides a three-phase structure composed of a mobile amorphous fraction equal to 0.41_3, a crystallinity of 0.27_7, and a rigid amorphous fraction of 0.31_0. Similar to many other polymers, *cis*-PBD displays multiple melting after isothermal crystallization, and up to three main endotherms can be evidenced by calorimetry, in dependence of the scanning rate. The results of conventional and temperature-modulated calorimetry analyses presented in this contribution suggest a link between multiple melting and devitrification of the rigid amorphous fraction in *cis*-PBD. The small endotherm located a few degrees above the crystallization temperature appears to be caused by concurrent partial mobilization of both the crystal and the rigid amorphous portions. Additional partial mobilization of rigid amorphous segments seems to take place at around −11 °C, and it is only above this temperature that large reorganization of the crystal phase becomes possible, allowing partial melting and recrystallization/annealing/crystal perfection.

1. Introduction

Polybutadiene (PBD) is the second largest volume synthetic rubber produced, next to styrene-butadiene rubber. The major use of PBD is in tires with over 70% of the produced polymer going into treads and sidewalls [1].

Polybutadiene is a homopolymer of 1,3-butadiene. It is polymerized by a solution process, using either a transition metal complex or an alkyl metal as catalyst [2]. At present, systems based on neodymium compounds are the most promising for the synthesis of *cis*-1,4-polybutadiene, since polymerization initiated by these catalysts is environmentally safe and the resultant rubber contains a high amount of 1,4-*cis* units and exhibits good technological characteristics [3].

Depending on the catalyst used and on the polymerization process, PBD with different stereoregularity can be produced. The different chain structures and configurations lead to corresponding variations in the thermal properties. Both *cis* and *trans* polybutadienes are semicrystalline polymers. The crystal structure of *cis*-1,4-polybutadiene has a monoclinic unit cell [4], whereas the *trans* isomer displays polymorphism, as its crystals can grow in a monoclinic as well as in a pseudo-hexagonal modification, the latter being in a condis state [5]. The thermal properties of polybutadiene also depend on microstructure, the glass transition temperature being equal to −102 °C and −83 °C, and the equilibrium melting point equal to 12 °C and 164 °C for the *cis* and *trans* isomers, respectively [6].

Thermal analysis of both *cis* and *trans* polybutadienes discloses multiple melting behavior. The multiple melting of the *trans* isomer is affected by its polymorphism, whereas *cis*-1,4-polybutadiene goes on fusion directly from the fully ordered crystal to the melt, without changing its crystal modification [5].

A few articles appeared in the literature to describe the multiple melting of *cis*-1,4-polybutadiene [5,7–9]. The most thorough investigation was conducted by Collins and Chandler, who quantified the dependence of crystallization and melting temperatures of *cis*-PBD in dependence of the rate of heating and cooling [9].

It needs to be underlined that the main studies on melting of *cis*-PBD date back to the 1960s and were mainly conducted by Differential Thermal Analysis instruments (DTA), which can provide quantitative information only on transition temperatures. The current availability of new scientific instrumentations allows to gain more detailed and quantitative information on the thermal properties of semicrystalline polymers, compared to DTA. Of special interest is the update of available knowledge on the melting process, due to the complexity of this transition, that often results from the overlapping of a number of different transformations of the metastable crystal structure, including partial recrystallization, annealing, and perfection of the initial crystals [10]. A differential scanning calorimetry (DSC) trace can allow to identify the main parameters that characterize polymer melting, as well as to recognize the occurrence of reorganization processes of the crystal phase, generally connected to the presence of multiple endotherms or exotherms, or to identify the existence of different crystal

* Tel./fax: +39 081 867 5059.
E-mail address: marialaura.dilorenzo@ictp.cnr.it

0032-3861/$ – see front matter © 2008 Elsevier Ltd. All rights reserved.
doi:10.1016/j.polymer.2008.11.025

morphologies from the position and breadth of the melting peaks. Additional quantitative data on polymer melting can be obtained by temperature-modulated calorimetry (TMDSC), that, in the quasi-isothermal mode of operation, permits to monitor slow changes in crystallization, melting, or crystal-perfection, each one resulting in a corresponding variation of the measured signal.

Quantitative data on fusion, discussed in this contribution for a commercial *cis*-1,4-polybutadiene grade, are needed to gain insight into the complex nanophase structure of semicrystalline polymers, in order to fully understand the processes related to the formation and evolution of the various nanophases that have been, at present, clarified only in part. Early investigations based their description of semicrystalline polymers on a two-phase model, where the two phases, one amorphous and one crystalline, have nanometer dimensions in one or more directions. Actually it is known that the decoupling between crystalline and amorphous phases is most often incomplete, due to the length of polymer molecules, much higher than the dimensions of the nanophases, as well as to possible geometrical constraints, which cause the coexistence of different types of amorphous fractions in semicrystalline polymers.

The different amorphous fractions are usually classified on the basis of their mobility. The unconstrained amorphous phase, that relaxes at the glass transition (T_g), is usually addressed as the "mobile amorphous fraction" (MAF), whereas the term "rigid amorphous fraction" (RAF) refers to the amorphous chain portions whose mobility is hindered by the near crystalline structures. The points of coupling between the amorphous and crystalline structures act as nanoscopic stress transfer, with remarkable effects on mechanical properties of the material, as recently demonstrated for isotactic poly(1-butene) [11].

Some influence of the rigid amorphous fraction on polymer melting behavior has been suggested in the literature. For isothermally crystallized poly(ethylene terephthalate), the endotherm appearing a few degrees above the crystallization temperature was proven to be caused by simultaneous partial fusion and enthalpy recovery of the rigid amorphous fraction [12]. For poly(phenylene oxide) it was shown that the physical state of the rigid amorphous fraction controls the onset of melting [13]. In this contribution the influence of the thermal properties of the rigid amorphous fraction on the overall multiple melting behavior of a commercial *cis*-1,4-polybutadiene PBD is discussed, based on quantitative DSC and TMDSC analyses.

2. Experimental part

2.1. Materials

cis-1,4-Polybutadiene was kindly provided by Polimeri Europa, S.p.A. (Ravenna, Italy). It is a commercial grade containing 97% of *cis* units and a low degree of branching. A certain amount of branches is generally incorporated in the main chain of commercial *cis*-PBD grades, since an extremely high linearity of polymer chains results in a too high cold flowability [3]. The used PBD grade has $M_w = 380{,}000$ Da and $M_n = 100{,}000$ Da. The polymer was used as-received, without further purification.

2.2. Calorimetry

DSC and TMDSC measurements were conducted with a Mettler DSC 822^e, Mettler-Toledo, Inc. Dry nitrogen was used as purge gas at a rate of 30 ml/min. Cooling was accomplished with the liquid-nitrogen accessory for the Mettler DSC 822^e. The temperature of the calorimeter was calibrated with the onset of the transition peaks for indium, naphthalene and cyclohexane. The heat flow rate was initially calibrated with the heat of fusion of indium, then refined with a baseline run of two empty aluminum pans and a calibration run with sapphire as a standard [14]. A correction for the heating rate is included in the Mettler-Toledo Star^e software (Tau Lag calibration) used for experiments and analysis.

In order to set the structure for the analysis of melting behavior, each PBD specimen was maintained at 70 °C for 3 min, then cooled at −30 °C/min to the crystallization temperature $T_c = -26$ °C, where it was allowed to crystallize for 1 h. After isothermal crystallization PBD was cooled at −10 °C/min to −130 °C, equilibrated at −130 °C for 3 min, then heated until complete melting using either a constant scanning rate, ranging from 1 to 20 °C/min, or a modulated temperature profile.

The TMDSC program was designed using the Star^e software of Mettler-Toledo, Inc. The experimental parameters were chosen to ensure linear thermal response and stationary conditions at least outside the transition range [15]. The underlying heating rate and modulation period were selected within the limits allowed by the commercial calorimeter used. The temperature amplitude and sample mass were sufficient to allow a good signal-to-noise ratio and at the same time not too large to reduce as much as possible thermal gradients within the sample. Non-isothermal TMDSC data were gained using a sawtooth oscillation with a temperature amplitude (A_T) of 0.2 °C, an underlining heating rate (q) of 1 °C/min and modulation periods (p) of 60, 90, and 120 s. The quasi-isothermal program involved a modulation of 0.2 °C about the base temperature T_o, a period of 60 s, and stepwise temperature increments of 5 °C after 16 min at each T_o. Extended-time quasi-isothermal analyses of a duration of 5 h were conducted at selected temperatures after heating the polymer, isothermally crystallized at $T_c = -26$ °C for 1 h, from T_c to T_o at 1 °C/min. After completion of the extended-time quasi-isothermal experiments, the material was heated from T_o until complete melting at a scanning rate of 1 °C/min.

From TMDSC measurements the reversing specific heat capacity ($c_{p,rev}$) was derived from the ratio of the amplitudes of modulated heat flow rate ($A_{\Phi,n}$) and temperature ($A_{T,n}$), both approximated with Fourier series [16]:

$$c_{p,rev}(\omega, n, t) = \frac{A_{\Phi,n}(t)}{A_{T,n}(t)} \frac{K(\omega, n, t)}{mn\omega} \quad (1)$$

where t is the time, n the order of the harmonic, ω the base modulation frequency ($\omega = 2\pi/p$), m the mass of the sample and $K(n,\omega,t)$ the frequency-dependent calibration factor. The reversing specific heat capacity data reported in this contribution were obtained from the first harmonics of the Fourier series.

3. Results and discussion

3.1. Heating rate dependence of the melting behavior

The thermal analysis of *cis*-1,4-polybutadiene after isothermal crystallization at −26 °C for 1 h and cooling to −130 °C is shown in Fig. 1 in dependence of the heating rate. The apparent heat capacity (c_p) data of Fig. 1 are compared to thermodynamic c_p values of solid and liquid PBD as taken from the ATHAS Data Bank [6]. Enlargements of the plots of Fig. 1 in the melting and glass transition regions are presented in Fig. 2a and b, respectively.

The multiple melting behavior of *cis*-PBD is largely affected by heating rate. At the lowest heating rates, three major endotherms can be evidenced in the DSC plots, in addition to a broad and weak endotherm at low temperatures, located below the isothermal crystallization point, as shown in Figs. 1 and 2. It discloses reorganization of the structure settled below the isothermal crystallization temperature, $T_c = -26$ °C. The rearrangements involve higher latent heat exchanges for measurements conducted at lower heating rates, due to the longer time of analysis. An increase of the scanning rate (q) from 1 to 2 °C/min results in a shift of the first two

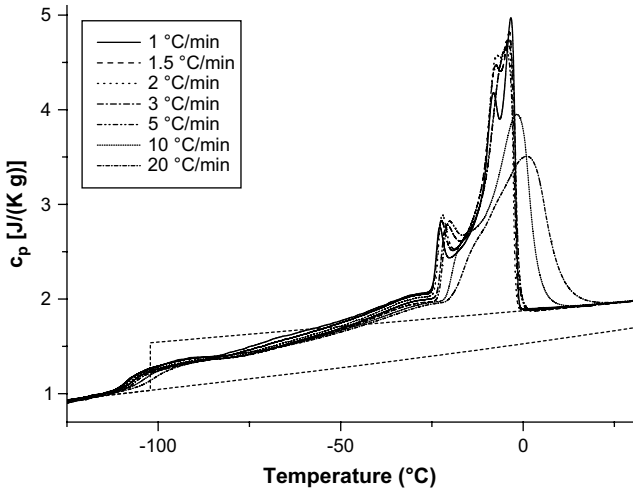

Fig. 1. Specific heat capacity of *cis*-PBD after isothermal crystallization at −26 °C and subsequent cooling, as measured upon heating at the indicated scanning rates. The specific heat capacity of the solid and liquid *cis*-PBD, shown as dashed lines, is taken from the ATHAS Data Bank [6].

major endotherms (T_I and T_{II}) to higher temperatures, and of the final fusion peak (T_{III}) to slightly lower temperatures. At faster heating rates the first endotherm still moves to higher temperatures with the increase of q, whereas the second and third peaks are not resolved and merge in a single endotherm whose position slightly moves to lower temperatures with the increase of heating rate, up to 5 °C/min. With higher scanning rates the whole melting range broadens and sensibly shifts to higher temperatures.

The DSC data shown in Figs. 1 and 2a provide valuable information on the different roles played by crystal reorganization and superheating on the overall fusion behavior of polybutadiene, revealed by the heating rate dependence of the apparent heat capacity curves. The position of the first two major endotherms (T_I and T_{II}) is affected by superheating and thermal lags' effects, as both move to higher temperatures with the increase of scanning rate, whereas the T_{III} temperature decreases with the heating rate. This reveals that very limited or even no crystal perfection/thickening of the thinner and/or more defective crystals occurs during heating in the temperature range of T_I and T_{II}, as in such a case an increment of the temperature of the two endotherms would have been observed at low rates. Conversely, crystal thickening and perfection takes place in the temperature range between T_{II} and T_{III}, as probed by the increase in T_{III} temperature upon slow heating, due to the longer time available for these processes during the DSC scan.

The small peak (T_I) appearing in Fig. 2a a few degrees above $T_c = -26$ °C, that emerges as an isolate peak or as a shoulder in the global fusion endotherm in dependence of the scanning rate, is not peculiar of *cis*-PBD, being detected in several other semicrystalline polymers [12,17–20]. According to some authors, this endotherm, that is centered a few degrees above the crystallization temperature and is usually addressed as the "annealing peak", is due to the melting of thin lamellae formed during secondary crystallization [21–23]. Other authors instead associate this peak to enthalpy recovery linked to mobilization of the constrained amorphous segments or more generally to some process involved in devitrification of the rigid amorphous fraction such as, for example, release of the constraints exerted by the crystalline phase [17,18,24]. Enthalpy relaxation associated with devitrification of the RAF occurring at the lowest endotherm was suggested for a number of polymers, including isotactic polystyrene, polycarbonate, poly(phenylene sulfide), nylon 6 and poly(3-hydroxybutyrate) [18,25–28]. A study recently conducted on poly(ethylene terephthalate) probed that multiple processes involving both the crystalline and

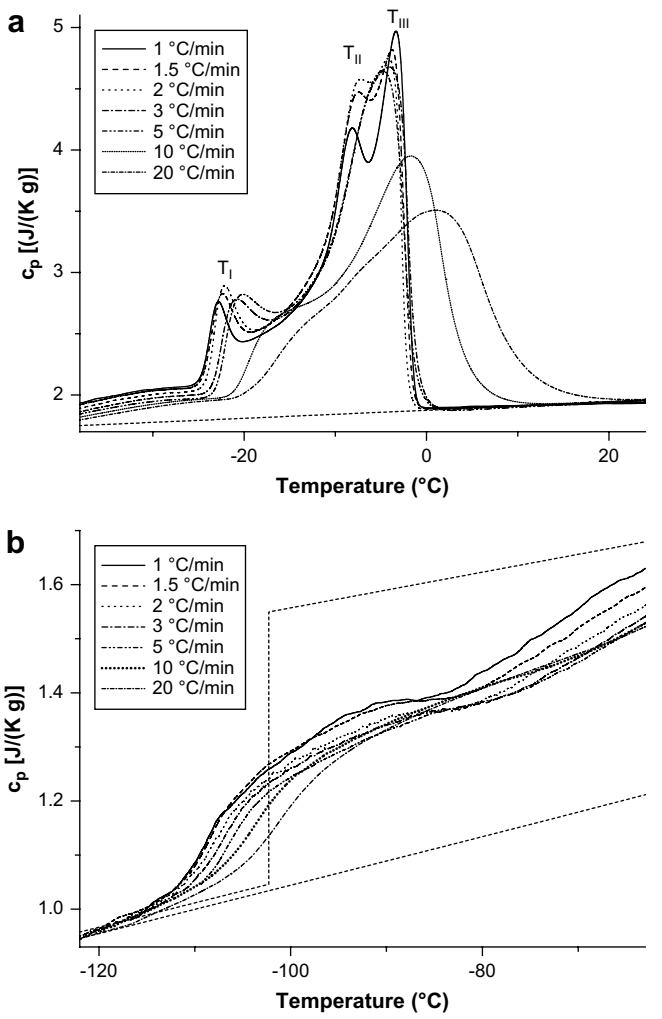

Fig. 2. Enlargement of the plot shown in Fig. 1: (a) melting region; (b) glass transition area. The major endothermic peaks are numbered in Fig. 2a.

the rigid amorphous fractions overlap in the temperature range of this small DSC peak, which results from the simultaneous occurrence of partial fusion of the crystals and enthalpy recovery connected to structural relaxation of part of the rigid amorphous fraction [12,29]. Similarly, for bisphenol-A polycarbonate it was shown that the constrained amorphous chain portions in the vicinity of secondary crystals, that melt at T_I, relax in part upon melting of the secondary crystals [25]. Upon heating, enhancement of chain mobility in the amorphous area favors fusion of thinner lamellae, which in turn reduces geometrical restrictions and allows release of strain in the interfacial area between the crystals and the surrounding amorphous regions. The DSC traces shown in Figs. 1 and 2a indicate that also in *cis*-PBD the rearrangements of the crystals that melt at T_I are hindered not only by constraints exerted by the neighboring crystallites, but also by possibly induced rigidity in the amorphous chain portions. Upon heating, the strained amorphous segments start to mobilize, allowing the onset of melting of the thinner and/or more defective crystals. A mutual influence of the two processes in the temperature range of T_I, probed for poly(ethylene terephthalate), polycarbonate and poly(3-hydroxybutyrate), seems to be active also for a rather flexible macromolecule like *cis*-1,4-polybutadiene. This explains the lack of improvement of the crystal phase at temperatures around T_I, crystal rearrangements being hindered by the coupled amorphous chain portions that are still vitrified.

As detailed below, the coupling between crystal and amorphous chain portions appears to determine the fusion behavior of *cis*-PBD also at higher temperature, in the T_{II} range, whose location also moves to lower temperature with the diminution of the heating rate in the DSC traces of Fig. 2a.

3.2. The three-phase structure

The heating-rate dependence of the experimental heat capacity of *cis*-1,4-polybutadiene in the glass transition region is exhibited in Fig. 2b, that presents an enlargement of the plot shown in Fig. 1. The specific heat capacity starts to deviate from thermodynamic c_p of solid polybutadiene at around −120 to −115 °C, in correspondence of the onset of the glass transition. The temperature range where T_g takes place depends on the heating rate, being shifted to higher temperatures with the increase of scanning rate, as typical for devitrification [10]. Additional thermal events overlap in this temperature range, and the overall heat capacity jump appears to be affected by the experimental conditions, making impossible to quantify the amount of amorphous phase that mobilizes at T_g by conventional DSC. To overcome this problem, temperature-modulated DSC analyses were conducted.

TMDSC data gained at the underlying heating rate of 1 °C/min at various frequencies of modulation are compared in Fig. 3 with the conventional DSC trace at the same constant heating rate of 1 °C/min. On the same figure, the reversing c_p plot of the quasi-isothermal TMDSC analysis in steps of 5 °C is also illustrated. As before, the experimental data are compared with thermodynamic c_p values of solid and liquid polybutadiene, as taken from the ATHAS Data Bank. Below the glass transition region and above completion of melting, DSC and TMDSC experimental data well agree with thermodynamic c_p of solid and liquid PBD, respectively. In the temperature region of the glass transition, a minor frequency-dependence of the reversing heat capacity can be observed. The dynamic T_g, i.e. the glass transition originating from temperature modulation and obtainable from the reversing c_p curve, is observed at temperatures slightly higher than the devitrification process derived from linear heating (thermal glass transition). This can be explained considering that the frequencies related to the ordinary linear heating rates are different from those used in TMDSC measurements, the latter being generally higher [30–32]. At completion of T_g, the reversing c_p curves gained by non-isothermal TMDSC data at three different frequencies and the quasi-isothermal reversing c_p data overlap, revealing the real extent of the transition, apart from non-reversing events that hinder correct determination of glass transition parameters of *cis*-PBD by conventional DSC.

Comparison of the data shown in Figs. 2 and 3 shows that non-reversing thermal events of endothermic nature in the glass transition region contribute to the apparent specific heat capacity measured by conventional calorimetry. The small endotherm overlapping T_g is ascribed to enthalpy recovery. Its magnitude increases with the decrease of heating rate, due to the more prolonged annealing during heating at slow rate [26,33]. Additional processes involving latent heat exchanges also overlap, and are more pronounced at slow heating rates, as seen in Fig. 2b.

It is important to note that TMDSC analysis is necessary for a quantitative assignment of the thermal events, which is not accessible by conventional DSC alone in the case of the glass transition of *cis*-1,4-polybutadiene, as probed by comparison of the DSC and TMDSC traces shown in Fig. 3. From the heat capacity jump of the reversing c_p curves of Fig. 3, a heat capacity step at T_g of 0.208 J/(K g) is measured, which, by comparison with the ATHAS Data Bank value of the glass transition of fully amorphous *cis*-polybutadiene, discloses a mobile amorphous fraction (w_A) equal to 0.41_3 after isothermal crystallization at −26 °C for 1 h and cooling to −130 °C. The crystal fraction as a function of temperature was computed from the conventional DSC plot gained at 1 °C/min, as a first approximation by assuming that a two-phase model, comprising only a crystalline and an amorphous fraction, is valid for PBD. This working condition involves the initial hypothesis that either no rigid amorphous fraction is present in the material, or that melting of PBD crystals takes place after full devitrification of the RAF. The crystal fraction (w_C) was obtained from eq. (2):

$$c_p(T) = w_C(T)c_{p,c}(T) + w_A(T)c_{p,A}(T) - [h_A(T) - h_C(T)]\frac{dw_C(T)}{dT} \quad (2)$$

where $c_p(T)$ is the measured specific heat capacity, $c_{p,C}(T)$ and $c_{p,A}(T)$ the thermodynamic values of the crystalline and mobile amorphous specific heat capacities and $[h_A(T) - h_C(T)]$ the heat of fusion, all tabulated in the ATHAS Data Bank [6]. Results of this analysis are presented in Fig. 4 that illustrates the evolution of crystal fraction with temperature during fusion. As suggested in Refs. [34,35], the

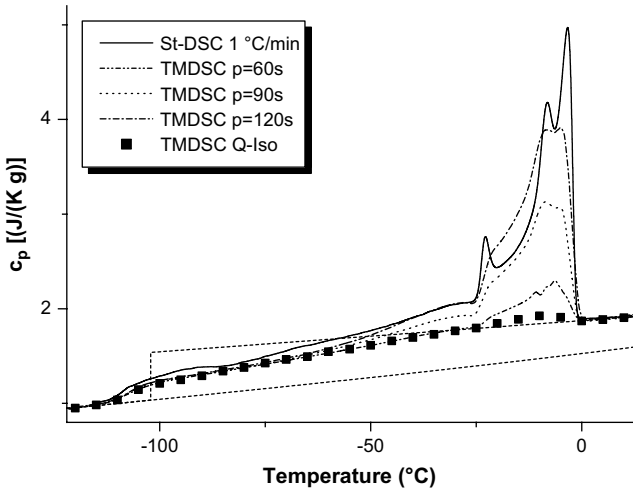

Fig. 3. Specific heat capacity of *cis*-PBD after isothermal crystallization at −26 °C and subsequent cooling, as measured upon heating at 1 °C/min. The thick solid line is the total heat capacity by conventional DSC, the thin lines are the reversing specific heat capacity measured by TMDSC at the indicated periods of modulation, the filled squares represent the reversing heat capacity after 16 min of modulation at each T_o. The specific heat capacity of the solid and liquid *cis*-PBD, shown as dashed lines, is taken from the ATHAS Data Bank [6].

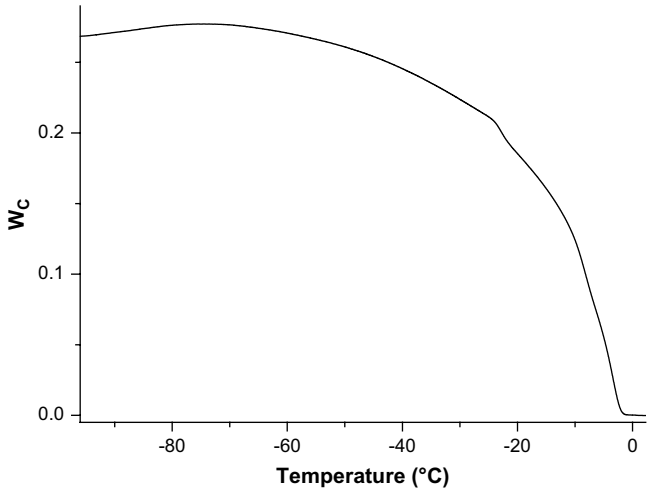

Fig. 4. Temperature dependence of the enthalpy-based crystallinity of *cis*-PBD during heating at 1 °C/min, calculated with eq. (2).

initial crystalline weight fraction of the material can be reasonably approximated by the maximum in the w_C vs. temperature plot, which points to a crystallinity $w_C = 0.27_7$. Comparison with the amount of mobile amorphous phase quantified by the heat capacity step at the glass transition probes that a considerable rigid amorphous fraction (w_{RA}) develops in *cis*-1,4-polybutadiene under the experimental conditions used, $w_{RA} = 0.31_0$. This value is probably underestimated, due to the above approximation in calculation of the crystal fraction, that neglects possible devitrification of the RAF in the melting range. No information on the kinetics of RAF devitrification can be provided by analysis of the reversing c_p plots shown in Fig. 3, that display a clear frequency dependence starting from about −85 °C, well below the reaching of the two-phase baseline, which is caused by reversing and non-reversing latent heat exchanges.

Very few data are available in the literature on the three-phase structure of *cis*-PBD. A previous article, reporting thermal analysis of a 100% *cis*-1,4-polybutadiene crystallized upon continuous cooling from the melt at rates ranging from 5 to 20 °C/min, points to a crystal fraction around 0.18–0.24, a mobile amorphous content of 0.65–0.80, and a rigid amorphous fraction (although not explicitly mentioned) ranging from 0.02 to 0.12 [5]. Due to different thermal history and molecular structure of the specific polymers, these data cannot be directly compared. However, the commercial material used in our study, that has a lower degree of chain regularity, develops much larger amounts of RAF compared to the 100% *cis*-PBD detailed in Ref. [5].

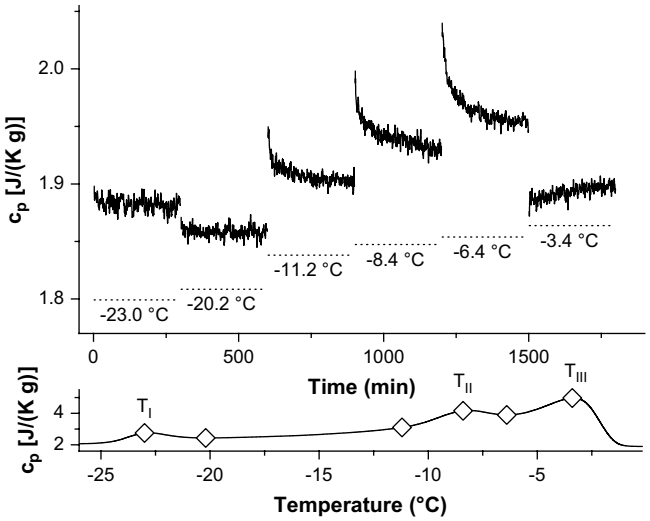

Fig. 5. Time dependence of the reversing specific heat capacity of *cis*-PBD during quasi-isothermal measurements at the indicated temperatures. The plots are shifted along the *x*-axis for clarity of presentation. The data are from separate measurements and are collected in a single graph in order to compare the reversing c_p trends for different T_os. The specific heat capacity of liquid *cis*-PBD, taken from the ATHAS Data Bank [6], is shown as dotted line for each T_o. The bottom part of the figure displays the experimental specific heat capacity of *cis*-PBD as measured by DSC at 1 °C/min. The squares on the c_p plot indicate the temperatures of quasi-isothermal modulation.

3.3. Quasi-isothermal TMDSC analyses

The data presented in Fig. 3 give information also on reversibility of the melting process of *cis*-PBD, and point to a small but sizeable reversible melting, which finds its maximum at around −10 °C, as indicated by the quasi-isothermal measurement conducted by modulating around the various base temperatures in steps of 5 °C. More quantitative data were gained by extended-time quasi-isothermal analysis. The chosen temperatures are those where maxima or minima in the apparent heat capacity vs. temperature plot, obtained by conventional calorimetry at a rate of 1 °C/min, appear. Results of these measurements, conducted by modulating around each base temperature for 5 h, are illustrated in Fig. 5.

Reorganization of the crystal phase in *cis*-PBD is strongly affected by the temperature of analysis. In the temperature range of T_I, at $T_o = -23.0$ and −20.2 °C, the reversing heat capacity decreases very slightly with time. At higher temperatures, where most of the fusion occurs, the reversing c_p plotted vs. time displays a more pronounced double exponential decay. For the quasi-isothermal experiment carried out by modulating around the peak temperature of the final endotherm, $T_o = -3.4$ °C, the apparent reversing c_p shows a quite unusual trend, increasing with time. In all cases, the measured reversing heat capacity, as well the reversing c_p values extrapolated to infinite times are higher that the thermodynamic c_p of totally liquid *cis*-PBD, that is reported in Fig. 5 for each T_o, probing reversible melting of this polymer.

Information on the variation of thermal stability of *cis*-PBD crystals upon prolonged exposure at the base temperatures of modulation is provided in Fig. 6, where the experimental heat capacity after 5 h of quasi-isothermal analysis is compared with the c_p vs. temperature plot that details the initial structure before the prolonged modulation. From these curves, the enthalpy-based crystallinity was derived, and the values after 5 h of permanence at each T_o ($w_{C,5h}$) are compared in Fig. 7 with the initial crystallinity of the material at the beginning of each quasi-isothermal experiment ($w_{C,o}$).

At all the analyzed temperatures some increase of crystallinity can be detected, which depends on the specific thermal treatment. The increase is considerable for the quasi-isothermal analyses conducted at temperatures −11.2 to −6.4 °C, in the region named T_{II}, where the second major endotherm of the DSC plot gained upon heating at 1 °C/min takes place. Some sizeable increase of the crystal fraction can be noted also when longtime modulation is conducted in correspondence of the peak temperature of the final melting endotherm (T_{III}), where the almost melted material undergoes significant recrystallization. Conversely, minor changes in crystallinity, close to the experimental error, are quantified for the quasi-isothermal measurements performed at the temperatures of the annealing peak ($T_o = -23.0$ to −20.2 °C).

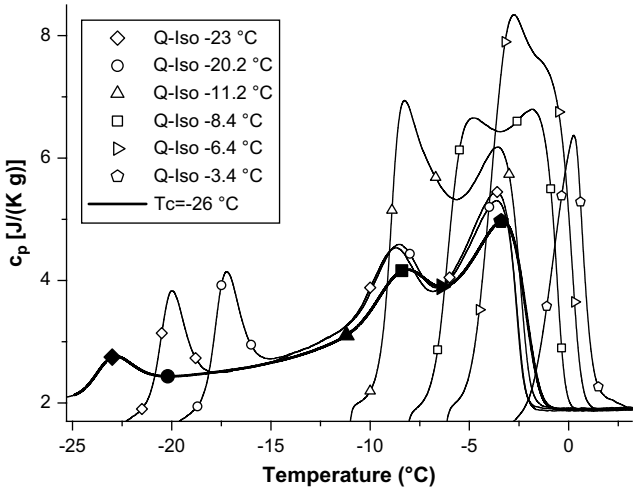

Fig. 6. Specific heat capacity of *cis*-PBD measured at 1 °C/min, after isothermal crystallization at −26 °C and subsequent cooling, followed by quasi-isothermal modulations for 5 h at the indicated temperatures. The thick solid line is the specific heat capacity of *cis*-PBD at 1 °C/min, after isothermal crystallization at −26 °C and subsequent cooling.

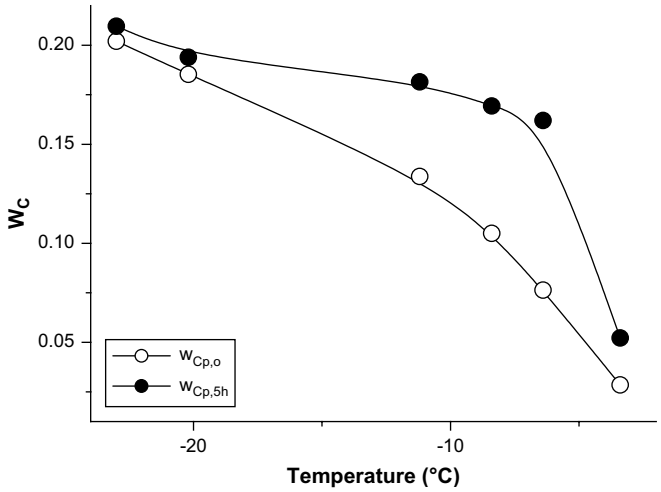

Fig. 7. Crystal fraction of *cis*-PBD before and after the quasi-isothermal analyses for 5 h.

As mentioned above, the trend of the reversing c_p plots varies with the temperature of analysis. Modulation in correspondence of the final endotherm (T_{III}) results in a continuous increase of the reversing heat capacity with time, as also seen in quasi-isothermal TMDSC of poly(butylene terephthalate) at high temperatures, very close or even above the initial melting point [36]. The prolonged experiment at $T_o = -3.4$ °C induces a sizeable enhancement of the crystal fraction, quantified in Fig. 7. The continuous increase of the reversing c_p trace with time of analysis arises from the higher crystal fraction that participates in the reversing melting process, despite the overall larger thermal stability of the material probed in Fig. 6.

The reversing heat capacity obtained by modulating at lower temperatures displays instead a double exponential decay, usually observed in semicrystalline polymers [37], more marked for the experiments conducted around T_{II}. The increase in crystallinity is considerable for modulations conducted around T_{II}, and minor for measurements performed at lower temperatures, around T_I. This corresponds to the fast and slow decays of the reversing heat capacity seen in Fig. 5 at T_os close to T_{II} and T_I, respectively. Comparison with the total c_p curves of Fig. 6, that depict the structure of the material before and after the quasi-isothermal treatments, reveals that only small changes in the thermal behavior are induced by the extended permanence around T_I, with only a sensible shift of the first endotherm to higher temperatures, and some minor influence on the two major peaks that move to slightly lower temperatures after the quasi-isothermal analysis. As mentioned above, the heating rate dependence of T_I indicates that this endotherm is caused by partial mobilization of the rigid amorphous fraction and simultaneous melting of the thinner and/or more defective crystals. The quasi-isothermal analysis shows the kinetics of these coupled processes, which overlap with partial recrystallization and concurrent additional vitrification of the amorphous phase. Both partial melting of the crystal phase and relaxation of the RAF produce an increase of the fraction of sample in the liquid state, whereas recrystallization and revitrification of the strained amorphous portions coupled with the recrystallized material contribute to a decrease of the baseline heat capacity. Overall, solidification slightly prevails, as probed by the small increase of the crystal fraction quantified in Fig. 7. The higher thermal stability of the perfected chain portions, whose melting point exceeds the amplitude of modulation, provides additional contributions to the slow decay of the reversing c_p.

It is important to underline that the main melting peaks, as well as the overall crystallinity, are only barely influenced by the prolonged stay at −23.0 and −20.2 °C, with large effects seen only in the shift of the first small endotherm (T_I). The development of crystals with improved thickness/perfection, occurring during the quasi-isothermal modulations, increases the thermal stability of the coupled vitrified amorphous segments that mobilize at higher temperatures in the subsequent DSC scan. It is likely that the gain in crystal perfection is limited by the concurrent possible partial vitrification of amorphous chain segments, and cannot go beyond the increase in melting temperature of a few degrees even after thermal treatments for rather long times, as demonstrated in Ref. [29] for poly(ethylene terephthalate). Conversely, the prolonged quasi-isothermal modulations around T_I seem to have no effect on the thermal stability of the primary crystals beyond that gained during the isothermal crystallization at −26 °C for 1 h, as proven by comparison of the locations of the T_{II} and T_{III} endotherms, that do not move to higher temperatures after the longtime modulations, as shown in Fig. 6. In addition, the crystals grown/thickened during the quasi-isothermal experiments, whose melting point (T_I) is located at higher temperatures, have less time to gain further perfection during the DSC scan than the original crystals, and melt at a slightly lower temperature. Overall, the limited reorganization of the crystal phase results in a small, but sizeable shift of the final melting endotherms to lower temperature values.

A minor variation in peak positions can be observed also after modulation at −11.2 °C, the temperature corresponding to the beginning of peak T_{II}. As illustrated in Fig. 6, in this DSC trace the endotherm T_I disappears and T_{II} becomes more intense and moves to slightly higher temperatures, whereas the location of T_{III} remains unchanged compared to the DSC scan obtained immediately after isothermal crystallization at −26 °C. It can be hypothesized that at −11.2 °C the constraints in the amorphous phase that allow large reorganization of the crystal phase are partly removed, as suggested by the slight shift towards high temperatures of endotherm T_{II} after the 5 h modulation, not noticed after the prolonged quasi-isothermal analyses at lower temperatures ($T_o = -23.0$ and −20.2 °C), but sensibly visible after modulation at higher temperatures ($T_o = -8.4$, −6.4, and −3.4 °C). Upon heating, the strained amorphous segments start to mobilize, allowing the onset of melting of the crystals that have reached the upper limit of their thermal stability, and can subsequently develop more stable structures. The considerable increase in crystallinity, caused by the prolonged exposure at each $T_o \geq -11.2$ °C supports the hypothesis that chain mobility is enhanced at $T \geq -11.2$ °C to levels that permit large extent of recrystallization and crystal perfection.

The results presented in this contribution for *cis*-PBD support the hypothesis, often appeared in the literature, of a close relation between the shape of DSC melting peak and devitrification of the rigid amorphous fraction. The small endotherm that is often seen a few degrees above the isothermal crystallization temperature was proven to contain contributions due to mobilization of the RAF for several semicrystalline polymers, like nylon 6, isotactic polystyrene and many others [12,18,24–28]. For poly(ethylene terephthalate) it was demonstrated that this small endotherm arises from devitrification of the RAF and partial melting, and that the two processes take simultaneously, being largely coupled [12]. For *cis*-PBD it is now shown that not only the first endotherm, as seen for other semicrystalline polymers, but also the overall multiple melting behavior is affected by the physical state of the RAF, since it is only in the temperature range of the second major endotherm that the rigid amorphous fraction attains sufficient mobility to allow development of perfected crystals with improved thermal stability that melt at T_{III}.

The cited literature data, together with the results detailed in this contribution, point to a coupled evolution of the various

nanophases in semicrystalline polymers. Melting of polymer crystals, as well reorganizations of the crystal phase, involving recrystallization/annealing/crystal perfection following partial melting, can occur only if the amorphous segment chains in proximity of the crystal/melt interface have sufficient mobility, which can achieved upon release of the strain of the amorphous chain segments coupled with the just melted crystals. These results here discussed for *cis*-PBD confirm the hypothesis appeared in the literature that in semicrystalline polymers the crystal phase must melt, at least partially, before the RAF can become mobile. Necessity for complete melting was seen in poly(phenylene oxide) (PPO), where mobilization of the RAF proceeds in parallel with disappearance of the crystals after sufficient mobility is achieved to permit crystal fusion [13].

However, these remarks cannot be taken as a general rule, as in some polymers no relation between crystal melting and relaxation of the rigid amorphous fraction could be proven. Isotactic poly(1-butene) can be cited as an example where mobilization of the RAF is completed at temperatures well below the onset of melting [11], thus showing no apparent relation between full mobilization of the amorphous phase with fusion. The latter example underlines that dissimilarities exist among the various semicrystalline macromolecules. Each polymer, due to its particular molecular structure, has specific peculiarities that determine its thermal behavior. Additional research effort is thus needed for a full understanding of the thermal behavior of the rigid amorphous fraction and its coupling with the other nanophases, in order to identify a possible common trend valid for all semicrystalline polymers.

Acknowledgements

The author wishes to thank Dr. Eng. Fabio Montanari and Dr. Eng. Salvatore Coppola of Polimeri Europa (Ravenna, Italy) for kindly providing the polybutadiene sample, Dr. Maria Cristina Righetti of IPCF-CNR (Pisa, Italy) for useful discussions, and Mr. Achille Taglialatela of ICTP-CNR for his assistance in literature search.

References

[1] Tate DP, Betea TW. Butadiene polymers. In: Mark HF, Bikales NM, Overberger CG, Menges G, editors. Encyclopedia of polymer science and technology. 2nd ed. New York: John Wiley and Sons; 1985.
[2] Yakovlev VA, Gavrilenko IF, Bondarenko GN, Chausova OV. Polym Sci Ser B 2006;48:203–5.
[3] Makovetskii KL, Yakovlev VA, Golenko TG, Bondarenko GN. Polym Sci Ser B 2006;48:61–5.
[4] Natta G, Corradini P. Angew Chem 1956;68:615.
[5] Grebowicz J, Aycock W, Wunderlich B. Polymer 1986;27:575–82.
[6] ATHAS Data Bank, http://athas.prz.rzeszow.pl/.
[7] Natta G, Moraglio G. Makromol Chem 1963;66:218.
[8] Mithcell JC. Polym Lett 1963;1:285–8.
[9] Collins EA, Chandler LA. Rubber Chem Technol 1966;39:193.
[10] Wunderlich B. Thermal analysis of polymeric materials. New York: Springer-Verlag; 2005.
[11] Di Lorenzo ML, Righetti MC. Polymer 2008;49:1323–31.
[12] Righetti MC, Di Lorenzo ML, Tombari E, Angiuli M. J Phys Chem B 2008;112:4233–41.
[13] Pak J, Pyda M, Wunderlich B. Macromolecules 2003;36:495–9.
[14] Archer DG. J Phys Chem Ref Data 1993;22:1441.
[15] Merzlyakov M, Schick C. J Therm Anal Calorim 2000;61:649–59.
[16] Androsch R, Moon I, Kreitmeier S, Wunderlich B. Thermochim Acta 2000;357–358:267–78.
[17] Xu H, Ince S, Cebe P. J Polym Sci Part B Polym Phys 2003;41:3026–36.
[18] Lu SX, Cebe P. Polymer 1996;37:4857–63.
[19] Lee Y, Porter RS. Macromolecules 1987;20:1336–41.
[20] Cheng SZD, Wunderlich B. Macromolecules 1988;21:789–97.
[21] Kong Y, Hay JN. Polymer 2003;44:623–33.
[22] Wang ZG, Hsiao BS, Sauer BB, Kampert WG. Polymer 1999;40:4615–27.
[23] Tan S, Su A, Li W, Zhou E. J Polym Sci Part B Polym Phys 2000;38:53–60.
[24] Song M. J Appl Polym Sci 2001;81:2779–85.
[25] Sohn S, Alizadeh A, Marand H. Polymer 2000;41:8879–86.
[26] Schick C, Wurm A, Mohammed A. Colloid Polym Sci 2001;279:800–6.
[27] Xu H, Cebe P. Macromolecules 2004;37:2797–806.
[28] Chen H, Cebe P. J Therm Anal Calorim 2007;89:417–25.
[29] Righetti MC, Di Lorenzo ML. e-Polymers, accepted for publication.
[30] Hensel A, Schick C. J Non-Cryst Solids 1998;235–237:510–6.
[31] Montserrat S, Calventus Y, Hutchinson JM. Polymer 2005;46:12181.
[32] Hutchinson JM, Ruddy M. J Polym Sci Polym Phys Edn 1990;28:2127–63.
[33] Hutchinson JM. Thermochim Acta 1998;324:165–74.
[34] Righetti MC, Tombari E, Angiuli M, Di Lorenzo ML. Thermochim Acta 2007;462:15–24.
[35] Righetti MC, Tombari E, Angiuli M, Di Lorenzo ML. Eur Polym J 2008;44:2659–67.
[36] Righetti MC, Di Lorenzo ML, Tombari E, Angiuli M. Macromolecules 2004;37:9027–33.
[37] Wunderlich B. Prog Polym Sci 2003;28:383–450.